Dynamic Surface Deformation of Cylindrical Bridge of High Prandtl Number Fluid in Oscillatory Thermocapillary Convection — Tspi Measuremet and G-jitter Effect —

By
K. Nishino[1], X. Li[1], Y. Kanashima[1] and S. Yoda[2]

Abstract: This report describes experimental studies conducted at Yokohama National University during 2003 JFY as a part of the Project Research on Marangoni Convection of National Space Development Agency of Japan (NASDA)[#]. The work consists of (1) the development of a new measuring method for dynamic surface deformation (DSD, hereafter) of cylindrical bridge of high Prandtl number fluid and (2) the study of g-jitter effect on DSD in a simulated g-jitter environment.

In the first work, a technique based on temporal speckle pattern interferometry (TSPI) is developed to make two-dimensional measurement of DSD in oscillatory thermocaplillary convection. The technique is designed to have a resolution of better than 0.1μm and be applicable to a curved liquid surface. Its performance is verified through a series of measurements targeting a flat mirror, a glass rod and a liquid bridge, all of which show dynamical surface displacement or deformation. The success of the measurement is due to the special phase-unwrapping algorithm devised for the measurement of oscillatory surface displacement or deformation.

In the second work, effects of g-jitter on the measurement of DSD caused by the oscillatory thermocapillary convection in a liquid bridge is studied experimentally. A vibration table driven by a piezoelectric actuator is constructed to generate g-jitters of realistic amplitude and frequency spectra. A micro-imaging displacement meter is used to measure DSD in the presence of g-jitter. It is shown that the natural DSD in the oscillatory state of thermocapillary convection is well separated in the frequency domain from that caused by harmonic and non-harmonic g-jitters. It is concluded that the DSD measurement in the future ISS experiment is feasible even in the presence of g-jitter there.

1. Development of DSD Measuring Technique Based on TSPI

1.1 Introduction

Electronic speckle pattern interferometry (ESPI) offers a versatile technique for measuring, with sub-micron accuracy, out-of-plane and in-pane displacements, vibrations, slopes and curvatures of optically rough surfaces, as summarized by Jones and Wykes (1983) and Rastogi et al. (2001). ESPI's advantages over other classical interferometric techniques lie in its relaxed requirement for reference surface, readiness of digital recording and so on. These features will also provide advantages for the measurement of specular and deformable surfaces such as liquid free surfaces. Unfortunately, ESPI has rarely been applied to such surfaces because they do not generate speckled wave fronts when illuminated by coherent light. This issue is, however, resolved by some methods. One idea is to let reference and/or object wave fronts impinge onto a rough surface placed in front of the camera.

---

[1] Yokohama National University, 79-5 Tokiwadai, Hodogaya-ku, Yokohama 240-8501, Japan
[2] Japan Aerospace Exploration Agency (JAXA), Sengen 2-1-1, Tsukuba-shi, 305-8505, Japan
[#] NASDA is now reorganized into Japan Aerospace Exploration Agency (JAXA).

Verga et al. (1998) used a ground glass to generate speckled wave fronts for measurement of liquid surface deformation. Another idea is to illuminate liquid surface with speckled light as proposed by Roussev et al. (1999). They measured the shape of a thin liquid layer on a flat plate whose backside is roughened to generate speckled light. Speckle images generated by these methods can be analyzed with the same procedures as those developed for ESPI measurement of rough surfaces.

The present study aims at developing a technique based on ESPI that can be used for the measurement of micron-order motion of a deformable liquid free surface. Our specific target is a quasi-cylindrical surface of a small liquid bridge, 2-5mm in diameter and 2-5mm in length, which is formed between two coaxial disks heated differentially for generating thermocapillary convection. Figures 1(a) and 1(b) show respectively the disk apparatus and the side-view photo of the liquid bridge targeted in the present study. This particular fluid geometry has been studied extensively (e.g., Kamotani and Ostrach 1998) from a viewpoint of flow instability due to thermocapillarity. The instability occurs when the temperature difference between the disks exceeds a certain critical value, causing the onset of micron-order motion of the liquid free surface. The fact that the magnitude of surface displacement can be less than 1mm requires quite a sensitive measuring technique to be developed. We have chosen ESPI for this purpose not only because of its advantageous features mentioned above but also because of the presence of large surface curvature that would make application of other conventional interferometric techniques very complicated. This latter advantage is exploited by van der Auweraer et al. (2002) in their measurements of surface shapes of complex three-dimensional models. Verga et al. (1998) also developed an ESPI system for measuring deformation of comparatively flat liquid surface.

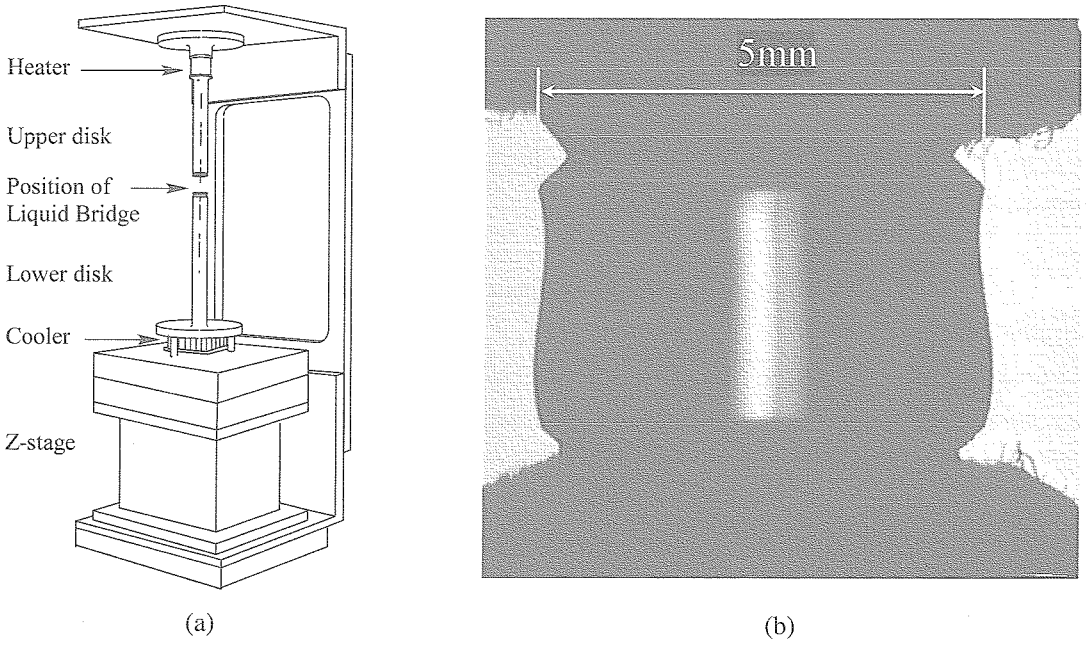

Fig. 1 Apparatus and photo of liquid bridge: (a) the disk apparatus for sustaining liquid bridge; (b) photo of liquid bridge's outline.

Phase extraction and phase unwrapping are the central issues in the development of ESPI as summarized in detail by Huntley (2001). It is in general impossible to make distinction between positive and negative displacements from a single pair of specklegrams, the problem inherent to any interferometric techniques. A remedy is the use of phase shifting, with which a series of predetermined phase shifts, either in temporal domain or in spatial domain, are added to the speckle field to be measured. A variety of techniques based either on temporal phase shifting (e.g., Nakadate and Saito 1985, Creath 1985) or on spatial phase shifting (e.g., Takeda 1990) have been proposed to date. As the phase extraction from such phase-shifted interferograms is usually made modulo 2π, the analysis should be followed by phase unwrapping, which is to resolve 2π ambiguity, to recover complete phase information. Obviously, a drawback of the phase-shifting techniques is their need for special hardware calibrated to give certain phase shifts, such as piezoelectric translators or diffraction gratings, to provide predetermined phase shifts to the speckle field to be measured. Another drawback in temporal phase shifting is that the target to be measured must be quasi-stationary during phase shifts being added, the requirement hardly accepted in the measurement of dynamic phenomena.

For measurement of dynamic displacement (or deformation), a new technique called temporal speckle pattern interferometry (TSPI) is proposed recently. This technique is based on the analysis of time-varying intensity of each speckle caused by continuous displacement of the surface. The intensity of speckle at an imaging sensor, $I(x, y, t)$, can be expressed as (e.g., Jones and Wykes 1983)

$$I(x,y,t) = I_b(x,y) + I_m(x,y)\cos\varphi(x,y,t) \tag{1}$$

where $I_b(x, y)$ and $I_m(x, y)$ are respectively the background and modulation intensities of specklegram at a position of (x, y) on the imaging sensor, and $\varphi(x, y, t)$ is the phase of intensity variation at an instant of t. It is assumed here that both I_b and I_m vary with time very slowly and thus they are regarded constant within the duration considered. When the displacement is unidirectional one (i.e., only either in positive or in negative direction), the intensity variation appears as a sinusoidal curve whose frequency is related to the rate of displacement. Joenathan et al. (1998) used a temporal Fourier analysis to extract phase information from such sinusoidally varying intensities to measure large deformations of more than 100μm. Hilbert transform can also be applied for phase analysis of such dynamic ESPI signal as Madjarova et al. (2003) presented. Li et al. (2001) proposed a new method, called time sequence phase method (TSPM), which analyzes time-varying speckle intensities to retrieve unwrapped phase information directly. They demonstrated that the proposed method was applicable to a continuous, unidirectional displacement of the test surface. Li and Tao (2002) extended this technique in order to measure surface vibrations. The extension is based on the detection of recurvature points (RPs), which appear in the time-varying speckle intensity at instants when the vibrating surface changes its direction of displacement. For the validation of their technique, Li and Tao chose an edge-clamped circular plate vibrating in a sinusoidal waveform at 0.1838Hz in frequency. As mentioned in their paper, this simplicity of vibration presented little difficulty in the detection of RPs in the validation measurement. Furthermore, Li et al. (2002) applied their TSPM successfully to the measurement of large deflection of thin films, demonstrating that the measurement of deflection of about 1400μm was possible with sensitivity of $\lambda/2$ or $\lambda/4$, where λ is the wavelength of the illumination beam used.

In this report, we report a TSPI technique for measuring micron-order dynamic displacement of deformable liquid free surface in quasi-cylindrical form as shown above. We have chosen an optical setup similar to that proposed by Verga et al. (1998) to make measurement of liquid surfaces. As shown later, a ground glass is placed at the image plane of an object lens. While Verga et al. used a fringe analysis for phase extraction, we have adopted TSPM proposed

originally by Li et al. (2001) because it has a potential of providing more spatially resolved information of displacement than the fringe analysis. Since dynamic displacements of liquid free surface should exhibit much more complicated features, such as those due to multiple modes, frequency harmonics, phase variations and so on, than the vibrating circular plate targeted by Li and Tao (2002), we have developed an automated and robust algorithm for detecting RPs from a set of consecutively acquired specklegrams. The algorithm is verified through a series of computer simulations using artificially generated specklegrams. The developed system and procedures are tested through a serial of measurements of dynamic surface displacement of both a flat mirror and a cylindrical glass rod, the latter providing a simplified model of the liquid bridge. Comparison data are taken with the laser focusing displacement meter (LFDM), which is commercially available for displacement measurement at a single point on the surface of little deformation. It is shown that time-varying displacements of those test surfaces measured with the developed TSPI system are in good agreement with those measured with the LFDM. The capability of the present technique is demonstrated by some experimental results taken from dynamic surface displacement of a liquid bridge of silicone oil.

1.2 Principle

This section gives a description of the principle of the present TSPI technique. Since the principle of ESPI is well documented in some previous literature (e.g., Jones and Wykes 1983 and Rastogi et al. 2001), it will not be repeated here.

Figure 2 shows a schematic of the present optical setup. The coherent laser beam is divided into reference and object beams by the polarizing beam splitter (PBS). It has about 95% reflectance for s-polarized component and 92% transmittance for p-polarized component. It is designed here that the s-polarized component serves as an object beam. The role of the $\lambda/2$ plate placed before the PBS is to rotate the polarization plane of the laser beam impinging on the PBS, thus to change the intensity ratio between s- and p-polarized components. The polarization direction of the object beam is rotated by $\pi/2$ when passing twice through the $\lambda/4$ plate inserted between the PBS and the object surface. This rotation results in 92% transmittance through the PBS when the object beam is in propagation toward the object lens, thus enabling the maximum use of laser beam intensity. This is important when the reflectance of the object surface is quite low as in the case of liquid surface. Both object and reference beams are recombined at the PBS and then imaged, by the object lens, onto the smooth-side surface of the ground glass. The rough-side surface of the ground glass is viewed by a CCD element through the camera lens. A polarizing filter is placed in front of the camera lens in order to accept only object and reference beams with the same polarization. As documented by Kihm (1997) and Ko et al. (2001), the use of ground glass is common in speckle photography for measurement of refractive index gradients. Joenathan and Torroba (1991) used a ground glass in their ESPI system to make displacement measurements insensitive to the angle of reference beam.

In the present setup, the complex amplitudes of the object and reference beams incident on a CCD array at (x, y) are given as,

$$A_{\mathrm{O}}(x,y) = a_{\mathrm{O}}(x,y)\exp\left\{i\left[\varphi_{\mathrm{O}}(x,y) + \varphi_{\mathrm{GO}}(x,y)\right]\right\}, \tag{2}$$

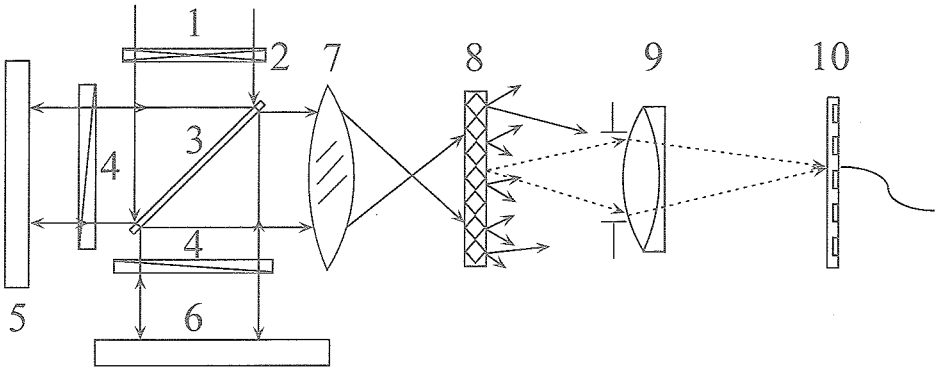

Fig. 2 Schematic of the present optical setup: 1, coherent laser beam; 2, λ/2 plate; 3, polarizing beam splitter; 4, λ/4 plate; 5, object surface; 6, reference surface; 7, object lens; 8, ground glass; 9, polarizing filter; 10, CCD camera's lens; 11, CCD element.

$$A_{\mathrm{R}}(x,y)=a_{\mathrm{R}}(x,y)\exp\left\{i\left[\varphi_{\mathrm{R}}(x,y)+\varphi_{\mathrm{GR}}(x,y)\right]\right\}, \tag{3}$$

where a_{O} and a_{R} are the amplitudes, φ_{O} and φ_{R} are the phases due to surface shapes, and φ_{GO} and are φ_{GR} the random phases introduced by the ground glass. Here subscripts O and R denote object and reference, respectively. The irradiance as a result of interference between the object and the reference beams is given by:

$$I_{\mathrm{F}}=|a_{\mathrm{O}}|^2+|a_{\mathrm{R}}|^2+2|a_{\mathrm{O}}|\cdot|a_{\mathrm{R}}|\cos\left[\varphi_{\mathrm{F}}\right], \tag{4}$$

where $\varphi_{\mathrm{F}}=\varphi_{\mathrm{O}}-\varphi_{\mathrm{R}}+\varphi_{\mathrm{GO}}-\varphi_{\mathrm{GR}}$ with (x, y) omitted for simplicity. This irradiance will generate speckles due to random phase modulation from $\varphi_{\mathrm{GO}}-\varphi_{\mathrm{GR}}$.

Any displacement of the object surface will result in the change of path length in the object beam. It is postulated here that the amount of displacement is so small that the object surface after displacement is relayed to the same position, within the resolution of each CCD array, on the ground glass. The change of path length is, therefore, determined by the change in the path between the object surface and the ground glass as follows:

$$A'_{\mathrm{O}}(x,y)=a_{\mathrm{O}}(x,y)\exp\left\{i\left[\varphi_{\mathrm{O}}(x,y)-\Delta\varphi(x,y,t)+\varphi_{\mathrm{GO}}(x,y)\right]\right\}, \tag{5}$$

where $\Delta\varphi$ (x, y, t) is the time-dependent phase change induced by the dynamic displacement of the object surface. Note that positive $\Delta\varphi$ corresponds to the displacement toward the CCD camera. The irradiance after the displacement then becomes

$$I'_{\mathrm{F}}=|a_{\mathrm{O}}|^2+|a_{\mathrm{R}}|^2+2|a_{\mathrm{O}}|\cdot|a_{\mathrm{R}}|\cos\left[\varphi_{\mathrm{F}}-\Delta\varphi\right]. \tag{6}$$

Equations. (1), (4) and (6) lead to the following relations:

$$I_b(x,y) = \left|a_O(x,y)\right|^2 + \left|a_R(x,y)\right|^2, \tag{7a}$$

$$I_m(x,y) = 2\left|a_O(x,y)\right| \cdot \left|a_R(x,y)\right|, \text{ and} \tag{7b}$$

$$\varphi(x,y,t) = \varphi_F(x,y) - \Delta\varphi(x,y,t). \tag{7c}$$

According to Wykes (1982), the phase change is related to the displacement of the object surface as follows:

$$\Delta\varphi = \frac{2\pi}{\lambda}\left(\vec{n_O} - \vec{n_S}\right)\cdot\vec{d}, \tag{8}$$

where $\vec{n_O}$ and $\vec{n_S}$ are respectively the direction cosines of the object beam and the reflected beam, $\vec{d}$ the displacement vector and λ the wavelength of the object beam. If the object surface is flat and illuminated normally by a planar wave front as in the present setup, Eq. (8) is simplified to

$$\Delta\varphi = \frac{4\pi}{\lambda}\left|\vec{d}\right|. \tag{9}$$

It should be noted that the angle between $\vec{n_O} - \vec{n_S}$ and $\vec{d}$ could vary if there is surface curvature as in liquid bridges. Such angle variation should be taken into account for accurate displacement measurement of curved surfaces.

Figure 3 shows an example of specklegram of a moving flat mirror surface taken at an instant, $t = t_0$. The

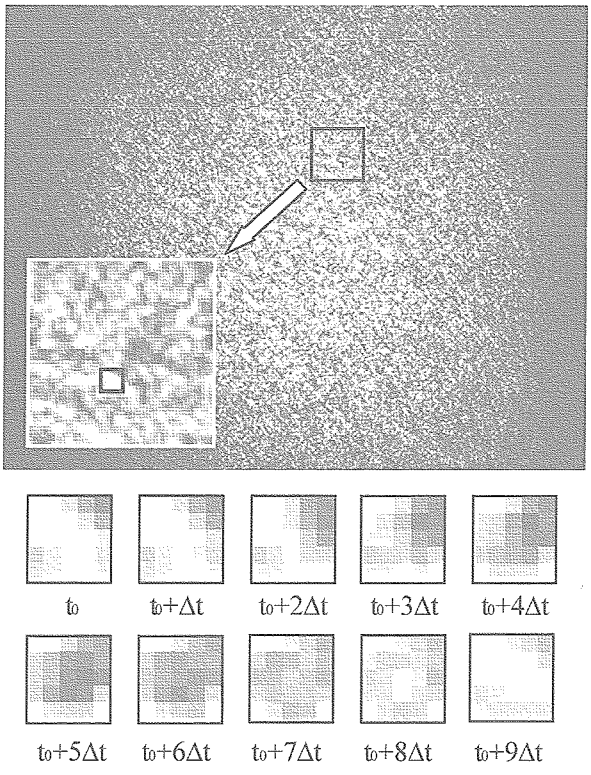

Fig. 3 An example of specklegram (only an area of 100×120 pixels shown) and time-varying intensity in a box marked (time interval Δt=1/60s).

details of image acquisition are described later in this paper. The local speckle intensities in the box marked vary with time as a result of dynamic surface displacement. Such a variation of speckle intensity (or gray level) at a pixel is illustrated in Fig. 4, where the displacement here is unidirectional one. The gray level varies periodically with time (or frame number) in accordance with Eqs.(6) and (7), thus generating a wrapped signal varying between I_{min} and I_{max}.

1.3 Phase extraction

1.3.1 Time sequence phase method

The time sequence phase method (TSPM) proposed by Li et al. (2001) consists of evaluation of wrapped phase and subsequent phase unwrapping.

The method for phase evaluation in TSPM is basically the same as those used in other scanning phase methods (e.g., Vikhagen 1990, Wang and Grant 1995, Saldner et al. 1996, Carlsson and Wei 2000). From Eq. (1), the wrapped phase is evaluated modulo π as follows:

$$\varphi(x,y,t) = \cos^{-1}\left\{\frac{2I(x,y,t) - I_{max}(x,y) - I_{min}(x,y)}{I_{max}(x,y) - I_{min}(x,y)}\right\} \tag{10}$$

where $I_{max}(x, y) = I_b(x, y) + I_m(x, y)$ and $I_{min}(x, y) = I_b(x, y) + I_m(x, y)$. It is assumed that sequential specklegrams for a sufficiently long duration are available so as to permit evaluation of I_{max} and I_{min} from time-varying intensity at each (x, y).

As the value of φ determined from Eq. (10) is in the range of $[0, \pi]$, it must be unwrapped by considering appropriate integer multiple of π. The time-sequence analysis proposed by Li et al. (2001) carries out this unwrapping directly by examining three consecutive speckle intensities, $I(x, y, t_i - \Delta t)$, $I(x, y, t_i)$ and $I(x, y, t_i - \Delta t)$, acquired at a constant time interval, Δt. As shown in Fig. 4, those three consecutive speckle intensities are used to judge whether the intensity of interest, $I(x, y, t_i)$, lies on a downward branch or on an upward branch of the intensity variation. The phase is unwrapped as $\varphi_{uwp} = 2n\pi + \varphi(t_i)$ if the intensity is on the downward branch and as $\varphi_{uwp} = 2(n+1)\pi - \varphi(t_i)$ if it is on the upward branch, where n is the total number of cycles counted from the

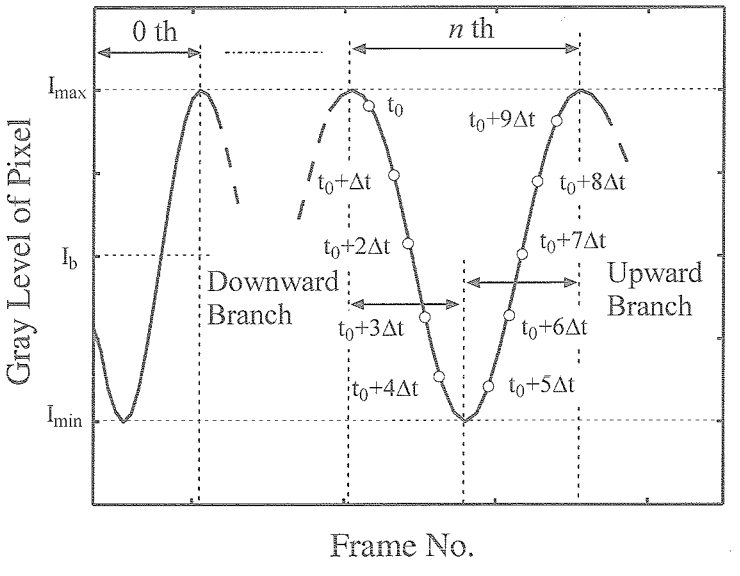

Fig. 4 Wrapped signal of speckle intensity corresponding to unidirectional displacement.

start of the measurement. The analysis relies on the condition that the recording speed is high enough to resolve at least five-six specklegrams in one cycle of intensity variation. Low-pass filtering is applied to remove intensity noises.

1.3.2 Detection of recurvature points

The time sequence analysis mentioned in the previous section is unable to distinguish positive displacement from negative displacement. Li and Tao (2002) improved this limitation in order to make measurement of surface vibrations with periodic change of displacement direction. Their improvement is based on the detection of RPs that appear in the intensity signal at instants when the surface displacement changes its direction. Li and Tao verified the proposed technique by measuring a circular plate vibrating with a single mode at a single frequency. However, their choice of such a simple vibrating displacement requires no elaborated algorithm for RP detection, and in fact they did not present any particular algorithms. However, in the measurement of dynamic displacement of liquid surface, an automated and reliable detection of RPs is needed because liquid free surfaces may exhibit complex modes of dynamic displacement.

In principle, RPs can be detected as local extrema in the intensity variation observed at each (x, y) as illustrated in Figs. 5(a) and 5(b), where the phase value of a simple oscillatory displacement is depicted in Fig. 5(a) and the corresponding gray-level variation is shown in Fig. 5(b). Two RPs appear in Fig. 5(b) at each instant when the dynamic deformation changes its direction. These RPs can be detected by means of numerical differentiation of the intensity variations. However, if their intensities are close to I_{max} or I_{min} as in the first RP in Fig. 5(b), they are not distinguishable from other local extrema corresponding to I_{max} or I_{min}. To deal with this problem, a new algorithm for RP detection is developed here. It is based on the assumption that the deformation

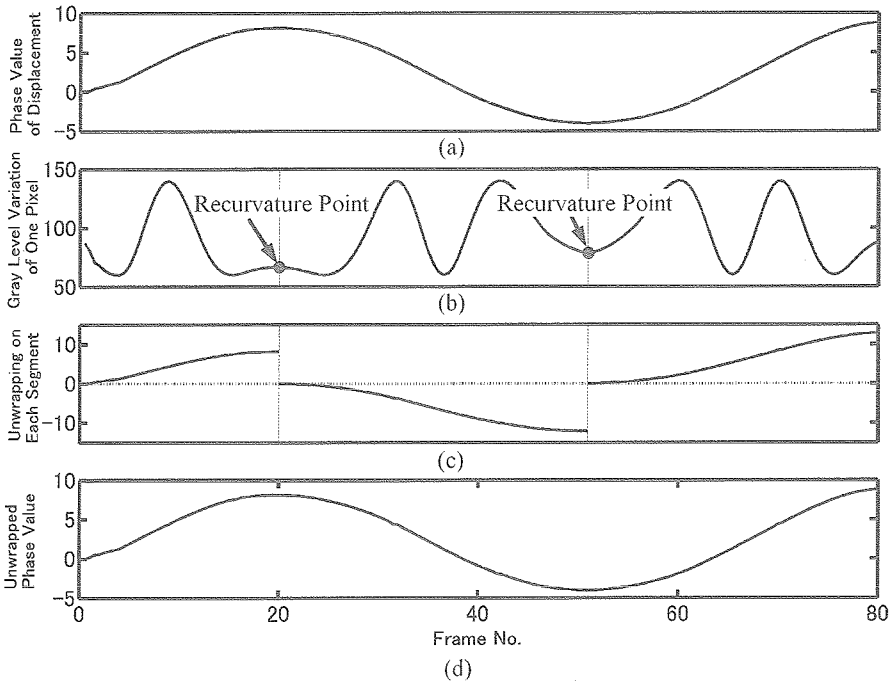

Fig. 5 Illustration of unwrapping procedures dealing with recurvature points: (a) time-varying phase value of displacement at a pixel; (b) corresponding gray-level variation showing two recurvature points; (c) segments of unwrapped phase value; (d) recovered phase value of deformation.

of liquid surface has a wavelength much longer than the average space between speckles. This assumption is reasonable in many cases of liquid surface deformation and allows us to expect simultaneous occurrence of RPs in neighboring speckles. This assumption is exploited as follows. Firstly, all extrema are detected from intensity variations of all effective pixels in the sequential specklegrams, where 'effective pixels' refer to those having modulation intensity higher than a prescribed threshold value denoted by I_{thresh}. Our experience shows that an average modulation intensity calculated from all pixels in the specklegrams can be used as I_{thresh}. To remove noises in the signals of intensity variation, the zero-phase digital filtering (Gustafsson 1996) is used. Secondly, a spatial window of $N_s \times N_s$ pixels in size is defined around an effective pixel of interest. Also a temporal window of $\pm N_f$ in frame number is defined around the instant considered to detect the extremum in the intensity variation of the pixel considered. This temporal window is to deal with possible phase jitter due to the noise present in the intensity signal. These spatial and temporal windows constitute a domain for the check of simultaneous detection of RPs in neighboring pixels. Lastly, the number of all extrema existing in this domain is counted. The number of extrema is denoted by N_e and the number of effective pixels in this spatial window is denoted by N_p. If $N_e / N_p \geq \alpha$, the extremum is registered as RP and otherwise as non-RP. Here, α is called the threshold for number ratio in this paper. The effect of the values of α, N_s and N_f on the detection of RPs will be discussed by means of numerical simulation in the next section.

Once all RPs are detected successfully, the change of direction of dynamic surface deformation is determined. That information is used for piece-wise phase unwrapping with the method described in the previous section as illustrated in Fig. 5(c). Finally, an overall phase unwrapping is completed by connecting the segments into a single curve as in Fig. 5(d). It should be mentioned that we still have no information about the initial direction of phase change, which must be determined separately. Carlsson and Wei (2000) proposed a method for determining the initial direction of phase change, which is based on the knowledge of the phase of neighboring pixels.

1.3.3 Computer simulations

The proposed algorithm for PR detection is verified through a series of computer simulations using artificially generated specklegrams. Subjective speckle fields are generated by using the method described by Kolenovic et al. (1999) in a simple configuration consisting of a rough surface, an imaging lens and a CCD element. A laser beam 532nm in wavelength illuminates the rough surface, where the mean roughness height of 10μm is assumed. The size of the illuminated area is $1.5 \times 1.5 mm^2$. The distance between the rough surface and the lens is 166.7mm. The lens has a focal length of 100mm and an aperture radius of 2.5mm. All these parameters are comparable to those of the present measurement system. The effect of reference beam is taken into account as a constant phase term added to the subjective speckle fields calculated. Random noises with root-mean-square intensity of 5 are added to the specklegrams generated, where each specklegram has an intensity ranging from 0 to 255 (8bits).

A series of three hundred specklegrams are generated from a rough surface with an assumed dynamic displacement as depicted in Fig. 6. The displacement ranges from 0 to 1.69μm, having a change of direction at 175 in frame number. The figure includes the generated specklegrams at some representative frame numbers. In the present computer simulation, the parameters in the algorithm, α, N_s and N_f are varied systematically to see their effect on the performance of the detection of RPs.

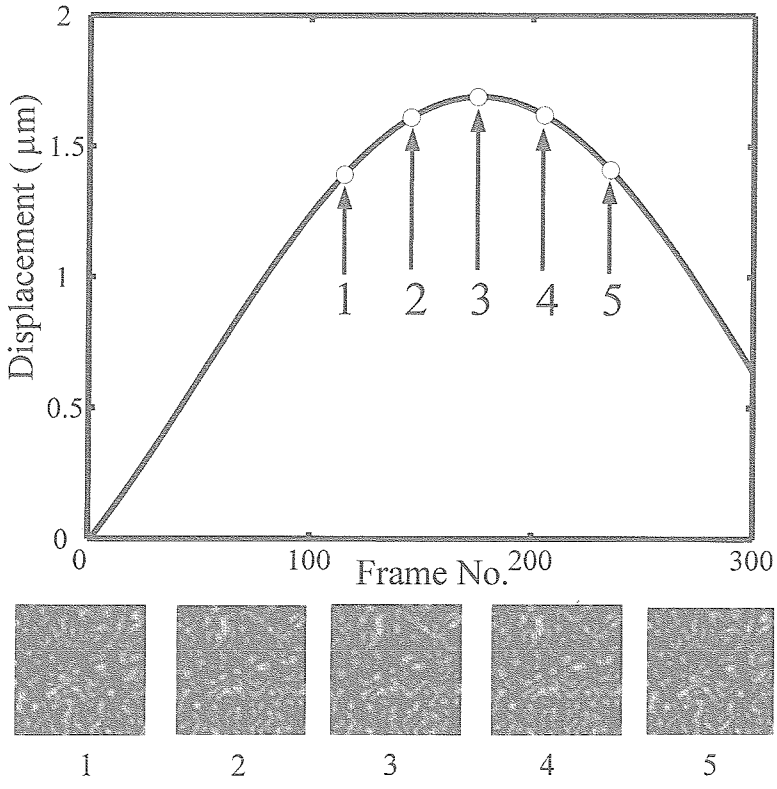

Fig. 6 Simulated displacement with a single change of displacement direction and artificially generated specklegrams at instants marked in the figure.

Figure 7(a) shows the success ratio of RP detection as function of α for different values of N_s and N_f, where the success ratio is defined as a ratio of the number of effective pixels with RP detected successfully to the total

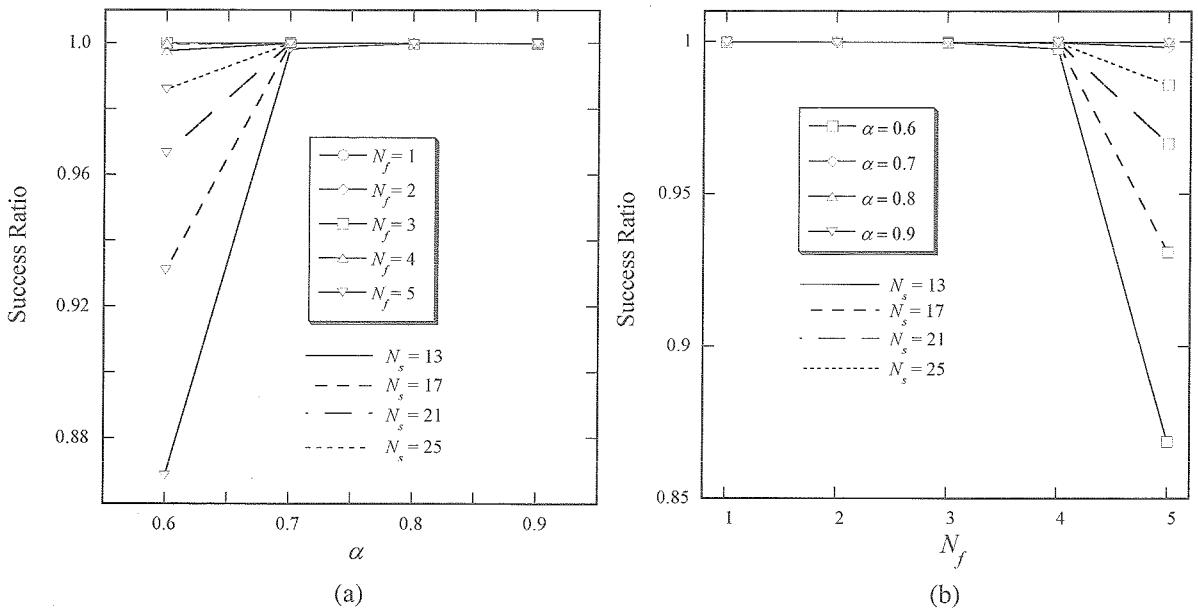

Fig. 7 Results of computer simulation: (a) effect of the threshold for number ratio, α, on the success ratio in the detection of recurvature points, (b) effect of the width of temporal window, N_f, on the success ratio in the detection of recurvature points.

number of effective pixels. Note that every effective pixel has a single RP in this simulation. The success ratio is satisfactorily high for α>0.7. Actually, it is 0.998 for α=0.8-0.9 regardless of the values of N_s and N_f. When α becomes smaller than 0.7, the success ratio starts to decrease, particularly for N_f = 5, with showing lower values for smaller N_s. Figure 7(b) plots the success ratio as function of N_f, showing considerable deteriorations at N_f = 5 and α=0.6. When N_f is large and N_s is small, the number of speckles observed in the spatial window can be small and consequently the local extrema corresponding to I_{max} or I_{min} within the domain (i.e., within the spatial and temporal windows) can happen to be in phase with each other. This will result in a spurious detection of RPs in the present algorithm. The results presented here suggest that (1) α should be larger than 0.6, (2) N_s should be as large as possible within requirement for the spatial resolution of the measurement, and (3) N_f should not exceed 5, particularly if smaller value of α is used (say, α=0.6-0.7).

1.4 Verification experiments

1.4.1 Experimental setup

Figure 8 shows the layout of the present experimental system. A liquid bridge is formed in the gap between the upper and lower disks, both 5mm in diameter. In verification experiment, a glass rod of the same diameter is placed at the same position. A flat mirror provides the reference surface. The illumination is given by a diode pumped solid state laser that delivers a coherent TEM_{00} beam with an output power of 60mW and with wavelength of 532nm. The CW beam is divided into the reference beam and the object beam by the polarizing beam splitter after going through a $\lambda/2$ plate and a beam shaping lens. The beam shaping lens is an achromat lens with a focal length of 140mm and has a function of adjusting the angle of incidence on the object surface. The object lens placed between the object surface and the $\lambda/4$ plate is an aspherical lens with a focal length of 39mm and a diameter of 60mm. The selection of such an object lens with short focal length and large diameter is to maximize the size of measurement area by illuminating the cylindrical surface with an object beam of large

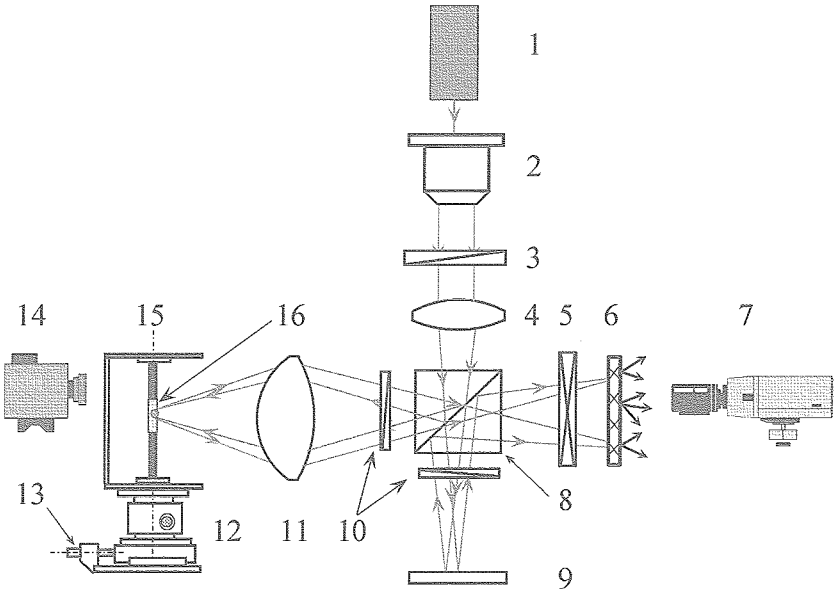

Fig. 8 Layout of the present experimental system: 1, laser; 2, beam expander; 3, $\lambda/2$ plate; 4, beam shaping lens; 5, polarizing filter; 6, ground glass; 7, CCD camera; 8, polarizing beam splitter ; 9, reference surface (flat mirror); 10, $\lambda/4$ plate; 11, object lens; 12, supporting stage; 13, PZT; 14, laser-focusing displacement meter; 15, main frame of liquid bridge; 16, cylindrical object surface (of glass rod or liquid bridge).

converging angle. In fact, if the illuminating beam were nearly collimated as in typical ESPI, the light reflected by the cylindrical liquid surface would become diverging and thus weakened, resulting in a very limited size of the measurement area. The measurement area achieved in the present setup is $0.7\times0.6mm^2$ of 5mm diameter cylindrical surface, which is quite satisfactory for the study of dynamic surface behaviors due to unsteady thermocapillary convection in the liquid bridge. The distance from the object lens to the object surface is adjusted to have a magnified image on the smooth-side surface of the ground glass.

A high speed B&W CCD camera with 512×480 pixels is used to image speckles generated at the rough-side surface of the ground glass. The camera is equipped with a telecentric lens having focal length of 55mm. A frame grabber with 512MB memory is used to capture specklegrams at 250fps for about 8 seconds consecutively.

In the present experiment, a piezoelectric translator (PZT) is installed in the liquid bridge apparatus to generate dynamic surface displacement in the out-of-plane direction. Its amplitude and frequency are controlled with a signal generator interfaced with a PZT driver. Since the amplitude and the frequency of the dynamic surface behaviors induced by the unsteady thermocapillary convection of interest are typically 1μm and 1Hz, respectively, they are set to 0.4-1.5μm in amplitude and 1-2Hz in frequency here.

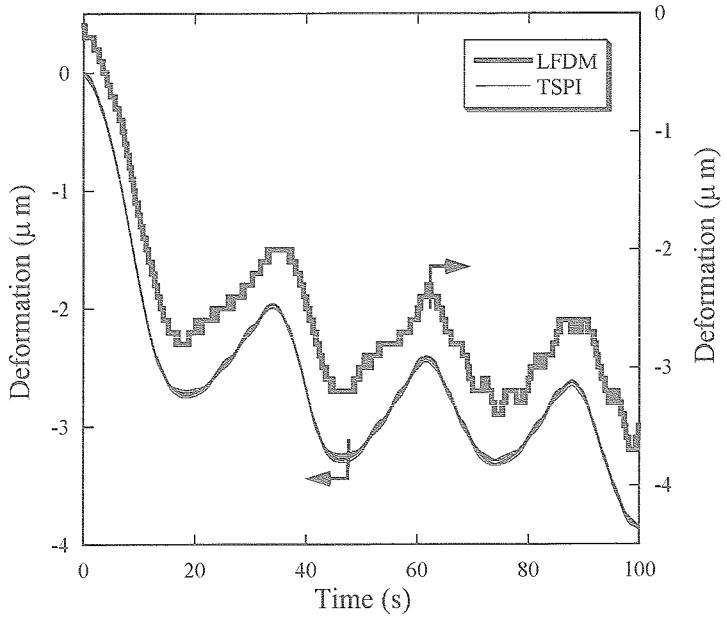

Fig. 9 Comparison of dynamic displacement of a flat mirror measured with the present TSPI and the LFDM.

The intensity ratio between the reference and object beams must be adjusted carefully to make the modulation intensity, I_m, as high as possible. The adjustment can be done efficiently by activating the PZT to move the object surface back and forth. At first the modulation intensity is estimated by directly looking at local intensity variations on a TV monitor during motion of the object surface, and this information is used to optimize the beam intensity ratio by rotating the λ/2 plate. The final adjustment is made by recording several sets of specklegrams with slightly different beam intensity ratio and by evaluating modulation intensity for each setting.

The LFDM is used simultaneously to measure the displacement for comparison. It emits a laser beam that is focused on the surface as a spot 2 μm in diameter and measures out-of-plane displacement with a resolution of 0.1μm. The LFDM is placed behind the object surface to measure the displacement of its backside.

1.4.2 Flat mirror surface

The first verification is done by measuring slowly moving surface of a flat mirror. In this experiment, the aspherical object lens is not used but the beam shaping lens is placed between the PBS and the ground glass as an object lens. A series of 3000 specklegrams are taken at 30fps in each run of measurement. Out-of-plane displacement is given by heating and cooling of a micrometer head of the supporting stage, instead of using the PZT. It should be mentioned that the CW laser used for this preliminary experiment is not the one used currently (output energy of 60mW) but the one used for long and thus with lower effective output energy (25mW). This should be the reason for comparatively worse (but still satisfactory) results from the flat mirror surface than those from the glass rod described in the next section.

Figure 9 presents the result taken under the heating/cooling sequence. It begins with cooling and thus with negative displacement. This information is used to avoid the ambiguity in the initial direction of displacement.

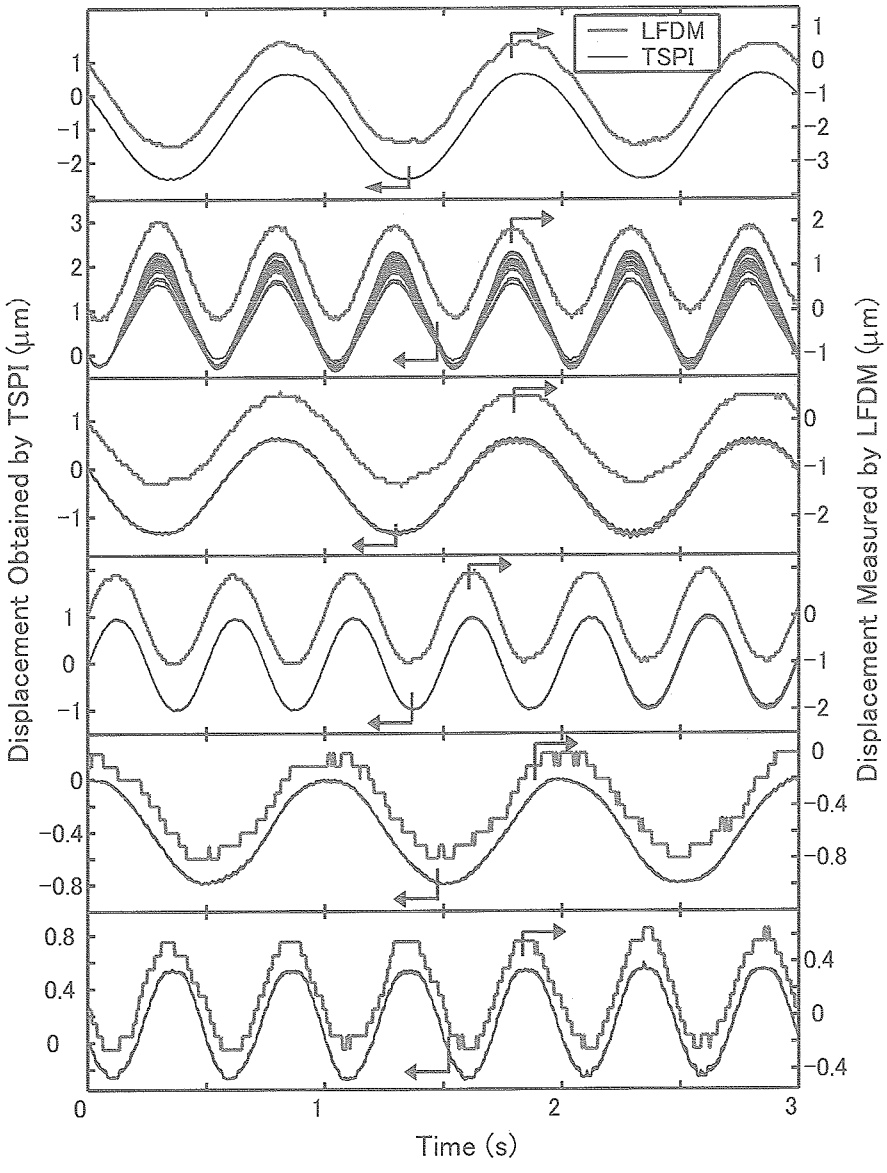

Fig. 10 Comparisons of dynamic displacements of a glass rod measured with the present TSPI and the LFDM: (a) case A, (b) case B, (c) case C, (d) case D, (e) case E, (f) case F.

The values of 0.8, 21 and 3 are used for α, N_s and N_f, respectively, in the RP detection algorithm, according to the simulation results described in Section 3.3. The data taken with the present TSPI system are indicated by thin lines and compared with the result taken with the LFDM indicated by a thick line. Note that the LFDM provides only a single point measurement while the TSPI provides measurements of all effective pixels, the number of which is about 111,000 in the present setup. The figure includes the TSPI data taken at 30 locations chosen arbitrarily from all effective pixels measured. As seen here, the agreement between TSPI and LFDM data is good for the whole heating/cooling sequence. Their difference defined as standard deviation is 0.12μm. Since this value includes measurement errors of LFDM, the standard deviation within the TSPI data is evaluated and it is 0.10μm.

Table 1 Evaluation of measurement results of glass rod surface.

	Case A	Case B	Case C	Case D	Case E	Case F
Amplitude (μm)	1.65	1.1	1.0	1.0	0.4	0.45
Frequency (Hz)	1.00	2.00	1.00	2.00	1.00	2.00
Error (μm)	0.075	0.180	0.085	0.089	0.039	0.038
Standard deviation (μm)	0.015	0.137	0.017	0.009	0.003	0.003

1.4.3 Glass rod

A glass rod made of BK7, 5mm both in diameter in length, is used for the measurement. The setup described in Section 4.1 is used to achieve the size of measurement area of 0.7×0.6mm^2. Figures 10(a)-(f) present comparison between the LFDM and the present TSPI for different oscillatory displacement conditions (i.e., amplitude and frequency) as summarized in Table 1. Those displacements are given by the PZT. A series of about 1000 specklegrams are captured continuously at 250fps for each measurement. Initial direction of displacement is determined from the data taken by the LFDM. The values of 0.8 and 21 are used respectively for α and N_s for all cases, while the values of N_f are 3 for Cases A to D and 5 for Cases E and F. Each figure includes TSPI data from 40 effective pixels randomly selected from the whole specklegram, where the modulation intensity of 25 is used to define the effective pixels. In the present experiments, the ratio of the effective pixels to the total pixels is always higher than 70%. The standard deviations between the TSPI data and the LFDM data are given in Table 1. They are well below 0.1μm except for Case B. The standard deviations within the TSPI data are also listed in the table. They are less than 0.02μm except for Case B. The reason for appreciably deteriorated (but still very satisfactory) result for Case B should be the instability of the laser that happens very occasionally.

The displacement is calculated from the unwrapped phase value through Eq. (9), which is simplified from Eq. (8) with neglecting the effect of surface curvature. This simplification is checked in Fig. 11, where the displacements measured at a total of 69 effective pixels located on diagonal lines crossing the whole FOV are plotted. It is obvious that there are no distinguishable discrepancies among the measurements. This indicates that the influence of the surface curvature can be neglected in the present measurement. This preferred feature is because the directional change of surface normal in the measurement area (0.7×0.6mm^2) is very small and it causes negligible effect on the displacement measurement (actually, the deviation is estimated to be less than 1%).

All the results shown in this section demonstrate well the validity and the accuracy of the present TSPI technique when applied to the measurement of dynamic displacement of cylindrical glass surface.

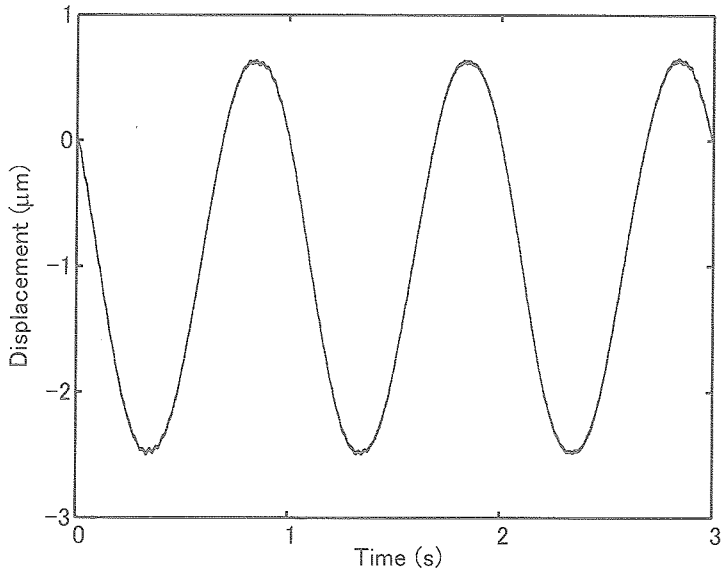

Fig. 11 Displacements of pixels on diagonal lines crossing the whole FOV of Case A.

Table 2 Evaluation of measurement results of liquid bridge surface.

	Case A	Case B	Case C	Case D
Amplitude (μm)	1.55	1.05	1.05	0.5
Frequency (Hz)	1.00	1.00	2.00	2.00
Error (μm)	0.162	0.138	0.152	0.073
Standard deviation (μm)	0.012	0.004	0.037	0.015

1.4.4 Liquid bridge

Four runs of measurement with different displacement amplitudes and frequencies are conducted as summarized in Table 2. The object lens is looking at the area near the upper disk. The size of the measurement area is $0.7\times0.6\text{mm}^2$ as before. The oscillatory displacement is given by the PZT and the comparison data is taken with the LFDM. Note that the frequency of displacement is low enough to guarantee that the whole liquid bridge is translated with the same amplitude. The values of the parameters for detecting RPs are $\alpha = 0.8$ and $N_s = 21$ for all cases, and $N_f = 3$ for Cases A to C while $N_f = 5$ for Cases D. The result for Case B is shown in Fig. 12(a) in the form of a three-dimensional surface plot of measured displacement. As far as we know, this is the first displacement measurement of two-dimensional surface area of liquid bridge.

Comparison with the LFDM for Case B is shown in Fig. 12(b). The standard deviation between TSPI and LFDM is 0.138μm, while that within the TSPI data is only 0.004μm. Agreement between the present TSPI and the LFDM is still satisfactory as in the case of the glass rod except that standard deviations between the TSPI data and the LFDM data are higher. It is reasonable since the object surface is a free liquid surface instead of a solid surface. Not shown here, the results for Cases A, C and D are similarly good and well compared with those measured with LFDM, as one can recognize from the values of standard deviation in Table 2.

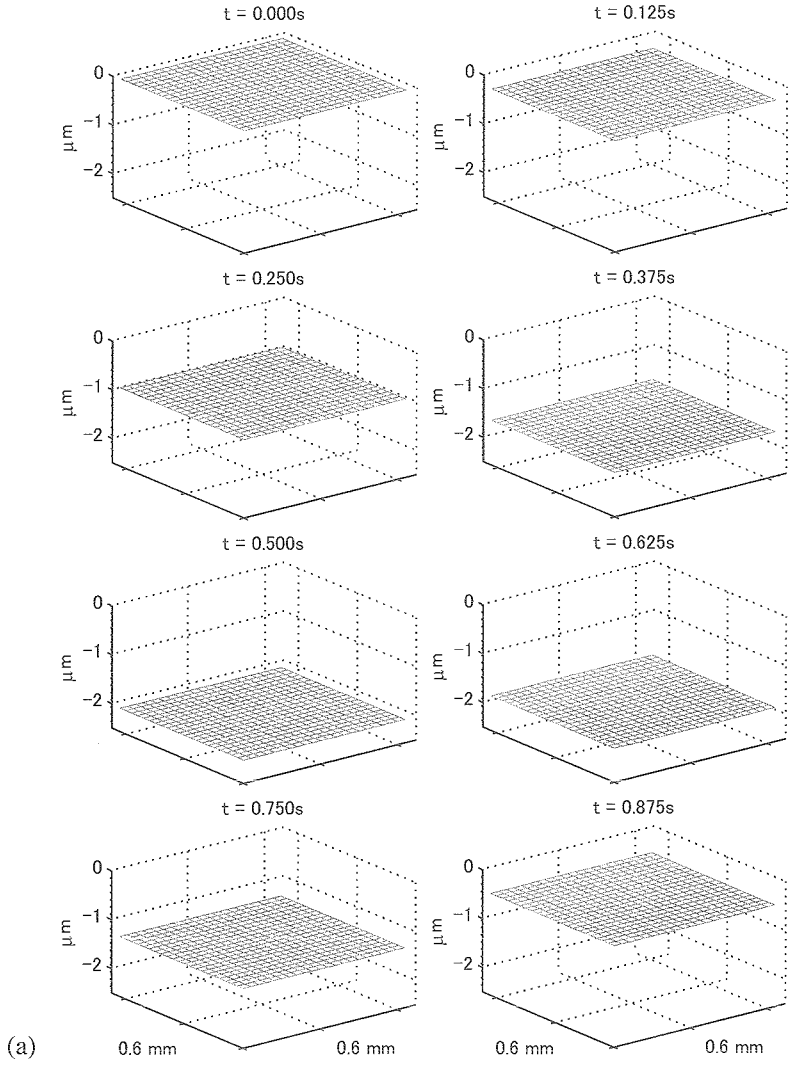

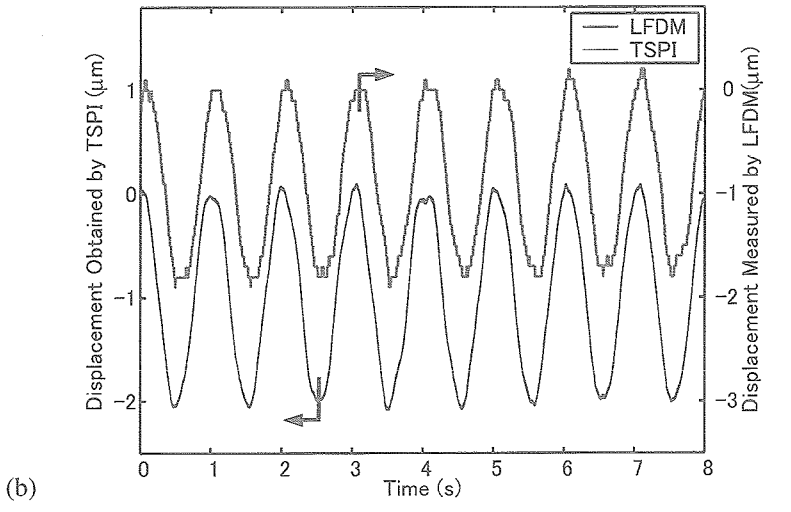

Fig. 12 Dynamic displacements of liquid bridge's surface measured with TSPI and LFDM:
(a) three-dimensional surface plots of displacement within the first second, and
(b) comparison of displacements obtained by TSPI and the LFDM.

1.5 Conclusions of Chapter 1

This chapter presents a technique based on temporal speckle pattern interferometry (TSPI), a recently developed version of electronic speckle pattern interferometry, for measuring micron-order surface motions of quasi-cylindrical liquid bridge. The time sequence phase method (TSPM) proposed recently has been extended to develop automated and robust procedures for phase unwrapping of time-varying speckle intensities generated from moving surfaces. The performance of the developed procedures is evaluated through a series of computer simulations made in a range of parameters involved. The technique is implemented into a TSPI system utilizing a ground glass for generating speckles from non-speckled reference and object wave fronts. Validity and accuracy of the technique are verified by the displacement measurement of oscillating surfaces of a flat mirror and a glass rod, where the detailed comparisons are made with a commercially available instrument for single-point displacement measurement. It is demonstrated that the present method is well applicable to the two-dimensional dynamic displacement measurement of a deformable surface of an actual liquid bridge.

2. Effect of G-jitter on the Measurement of DSD

2.1 Introduction

A liquid bridge suspended between two coaxial disks differentially heated is typical flow geometry for the investigation of flow instability of thermocapillary convection. When the temperature difference between the disks is small, a laminar state with an axisymmetric toroidal flow pattern appears in the liquid bridge. When the temperature difference is increased to exceed a certain critical value, ΔT_c, the flow and temperature fields start to oscillate. This onset of oscillation has been an extensive research target in theoretical, numerical and experimental work. High Prandtl number fluids, such as silicone oil, are usually used in the experiment.

Some recent studies (e.g., Kamotani et al. 2001) suggest that DSD of the liquid bridge of high Prandtl number fluid, particularly that near the hot disk, should play an important role in the transition mechanisms. This suggestion is based upon the experimental finding that the transition conditions for a wide range of liquid-bridge size are correlated well with a non-dimensional parameter representing "deformability" of the liquid bridge surface. The finding, however, seems to be in contrast with the assumption made in the past theoretical

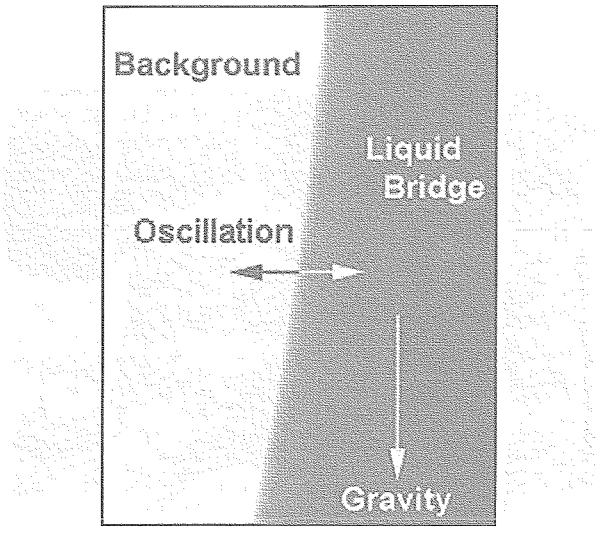

Fig. 13 Image of the edge of the liquid bridge seen in micro-imaging displacement meter (MIDM).

and numerical work, both based upon the governing equation neglecting the contribution of DSD. To clarify this issue, a microgravity experiment was proposed in response to the International Announcement of Opportunity in 2000 for microgravity experiments to be conducted in ISS. The proposal is now under consideration as a candidate for experiments to be conducted in the Fluid Physics Experiment Facility (FPEF) under development by JAXA.

In this proposed experiment, DSD of a liquid bridge will be measured with a microscopic imaging technique. As the DSD measurement can be influenced by g-jitter in ISS, the effect must be well examined. The present paper reports some results of the examination made in artificially generated g-jitter in the ground experiment. It is shown that a simple g-jitter table driven by a piezoelectric actuator can realize g-fluctuations of realistic magnitude in an adequate range of frequencies. It is also shown that the DSD component associated with the oscillatory state in the liquid bridge can clearly be distinguished, by means of appropriate filtering, from original DSD signals contaminated by the effect of g-jitter. This second result indicates the feasibility of DSD measurement in the proposed microgravity experiment in ISS.

2.2 Method

2.2.1 Micro-imaging displacement meter (MIDM)

A new technique for measuring dynamic surface deformation of liquid bridge is used here. It is based upon microscopic imaging of oscillatory motions of the edge of the liquid bridge illuminated by back lighting. A

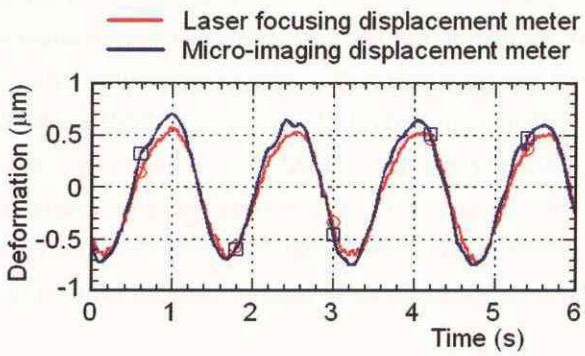

Fig. 14 Comparison of DSD measurement between the present MIDM and the laser focusing displacement meter (LFDM).

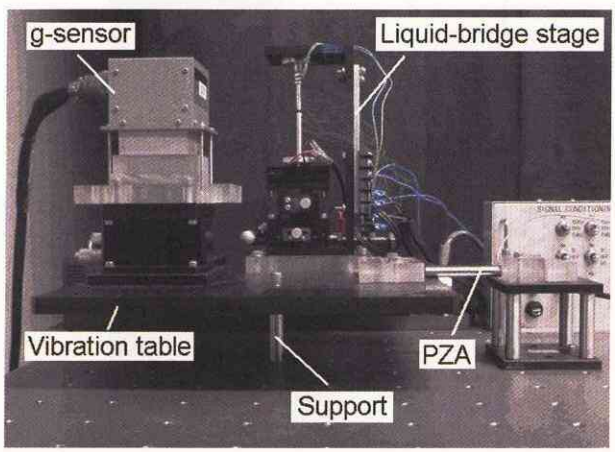

Fig. 15 Photo of the present vibration table driven by the piezoelectric actuator (PZA).

similar technique was used by Cao et al. (1991) and Yao et al. (1996), who, however, reported few details on the technique. The present technique, referred to as micro-imaging displacement meter (MIDM), consists of a black&white CCD camera (640×480 pixel) equipped with a microscope objective (Mitutoyo M Plan Apo 20×), a Xenon light source with a fiber light guide, and a frame grabber with 1 GB memory capacity. The microscope objective is characterized by its long working distance (30.5mm). The field of view is 410μm×325μm, giving a cell resolution of 0.65μm/pixel. As shown in Fig. 13, the liquid bridge taken with the camera appears as a black area in the white background. The DSD is observed as back-and-forth motion in horizontal direction in the image.

To detect the position of the edge of the liquid bridge, the edge-detection algorithm developed by Nishino et al. (2000) is implemented into the present MIDM. The edge detection is done along every horizontal line crossing the interface between the liquid bridge and the background. Averaging over eleven horizontal lines is taken to improve S/N of the detection. This leads the effective resolution of MIDM to become better than 0.1μm. Its temporal resolution is limited to 60fps presently by the framing speed of the camera. Figure 14 shows the comparison of DSD measurement between the present MIDM and the laser focusing displacement meter (LFDM). The latter is a commercially available instrument to measure DSD at a single spot (0.2μm) with a resolution of 0.1μm and it is applicable only to the liquid surface of little deformation. The agreement between MIDM and LFDM is quite satisfactory as recognized in this comparison. Further details of MIDM will be reported elsewhere.

2.2.2 G-jitter simulator

To generate g-jitter of realistic magnitude and frequency spectra in the ground experiment, a vibration table driven by a piezoelectric actuator (PZA) is constructed. The layout is shown in Fig. 15. The table is supported by a single metal rod. A liquid-bridge stage, a g-sensor and a CCD camera with a microscope objective (not shown here) are mounted on the table. The lowest resonance frequency of the table having those loads is measured to be about 170Hz, presenting no problem in the current g-jitter simulation conducted under 100Hz. The g-sensor has a resolution of 1μg and placed at the same height with the liquid bridge. The PZA used here achieves the maximum force of 800N and the maximum deformation of 60μg. It is capable of generating horizontal g-jitter of 15mg at 5Hz oscillation on the table.

The operation of the PZA is controlled by an analogue voltage supplier interfaced with a computer. A feedback control system using g-sensor signals is to be constructed to reproduce any desired frequency spectra of g-jitters on the vibration stage. In the present experiment, the g-jitter signal available at the web site of Principal Investigator Microgravity Services (PIMS) are used to determine the voltage given to the PZA. To do so, the g-jitter signal are integrated twice to obtain displacement signal that is then fed into the PZA by means of analogue voltage. Figure 16 shows the amplitude spectra of g-jitter from PIMS data and that generated and measured on the vibration table. Obviously, the generated g-jitter is different from PIMS data because of the non-linear property of the PZA used. Since the purpose of the present study is not to reproduce g-jitter identical to the PIMS data but to generate g-jitter with realistic amplitude and frequency spectra, the currently generated g-jitter is used to investigate their effect on DSD measurement. It should be mentioned that any frequency components of DSD higher than 30Hz are measured as lower frequency components as a result of aliasing in the present MIDM whose temporal resolution is 60Hz. This must be considered carefully in the interpretation of DSD measured.

2.2.3 Liquid bridge

A liquid bridge of silicone oil (5cSt) is suspended between two coaxial disks heated differentially. The upper disk is heated while the lower one is cooled to minimize the effect of buoyancy. The disk diameter, D, is 5mm, and the length of the liquid bridge, L, is 2.5mm, thus giving the aspect ratio of 0.5. The disk temperature is measured with thermocouples imbedded in the disks. The surface temperature of the liquid bridge is monitored with a fine thermocouple (25μm in diameter) placed near to but not in contact with the surface. The onset of oscillation is detected by the temperature signal from this thermocouple together with the DSD observed with naked eyes. The critical temperature difference, ΔT_c, is from 30 to 38K, depending on the ambient temperature. Yukawa et al. (2002) reported that a pulsating oscillation of 1.20Hz first appears and it then changes to a rotating oscillation of 0.95Hz at a slightly higher ΔT for the present conditions of liquid bridge. During DSD measurement, ΔT is kept constant to achieve a quasi-steady state of oscillation. The measurement of DSD is done at the middle height of the liquid bridge. Image acquisition is done for about 5s continuously.

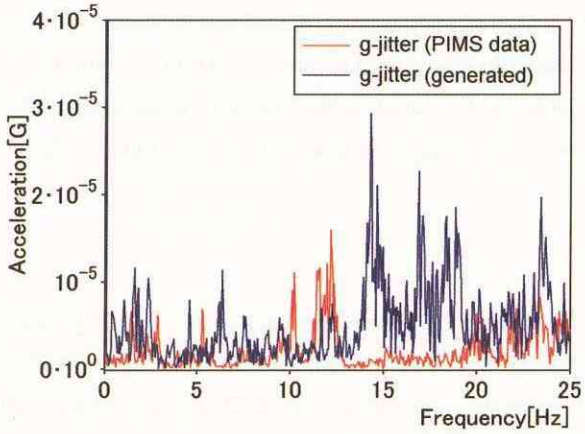

Fig. 16 Amplitude spectra of g-jitter from PIMS data and that generated and measured on the vibration stage.

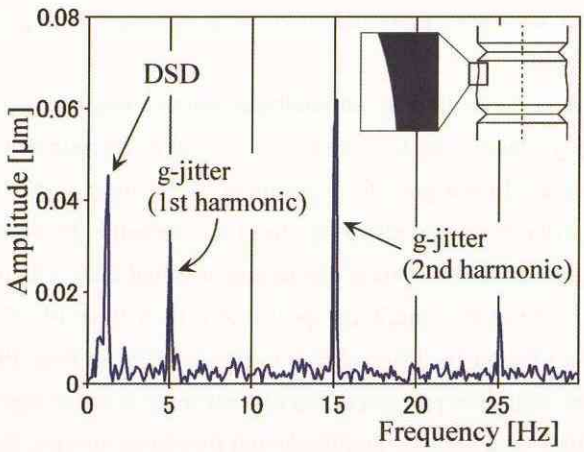

Fig. 17 Amplitude spectrum of DSD in the presence of harmonic g-jitter whose fundamental frequency is 5Hz.

2.3 Results and discussion

2.3.1 Harmonic g-jitter

The present experiment has begun with the imposition of harmonic g-jitter on the liquid bridge. Such harmonic g-jitters are generated by supplying sinusoidal voltage variations to the PZA. Sanz and Diez (1989) evaluated resonance frequencies of liquid bridge of inviscid fluid under the condition of no gravitational force. Their evaluation would predict resonance frequencies of 20.0, 7.3-11.5, 10.4-13.6, and 16.7Hz for modes of liquid-bridge oscillation for (m, n)=(0,2), (1,1), (2,1) and (3,1), respectively, where m and n are the azimuthal and axial modes of oscillation. It is found that the liquid bridge in the present experiment has a sensitive resonance frequency of about 15Hz, which might be corresponding to the one for (m, n)=(2,1) or (3,1) above. At this resonance frequency, the liquid bridge exhibits large DSD whose amplitude is much larger than that of natural DSD caused by the oscillatory state in the liquid bridge. However, the DSD components can be well discriminated in the plot of frequency spectrum as shown in Fig. 17. This result is obtained in the presence of harmonic g-jitter whose fundamental frequency is 5Hz. Since the g-jitter generated here has roughly triangular wave form rather than sinusoidal one, the odd multiples of the fundamental frequency appear as

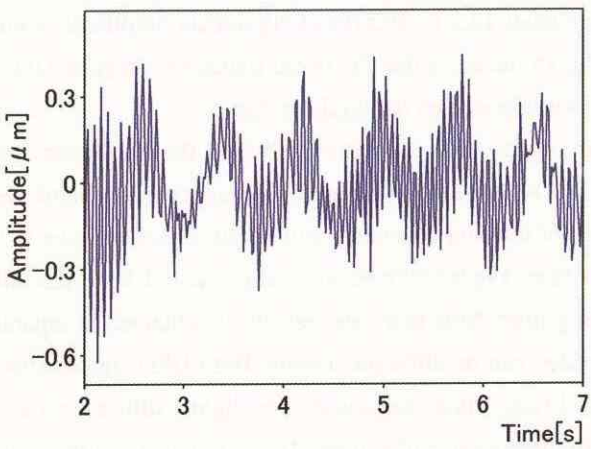

Fig. 18 DSD signal measured in the presence of non-harmonic g-jitters generated at ΔT=39K.

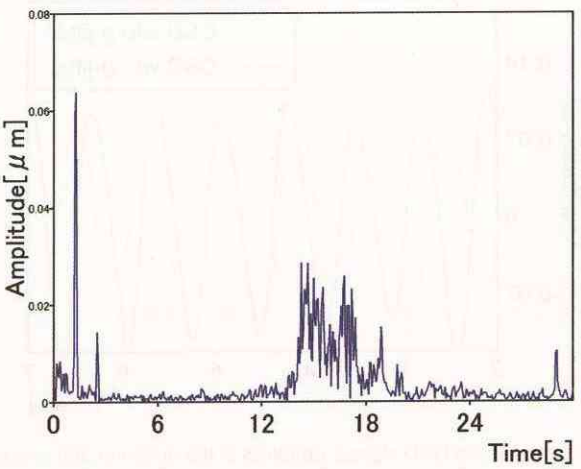

Fig. 19 DSD signal measured in the presence of non-harmonic g-jitters generated at ΔT=39K.

higher harmonics. It is seen in Fig. 17 that the natural DSD at about 1Hz is clearly recognized in the amplitude spectrum and it is well separated from other components of DSD generated by the g-jitter. This suggests that the natural DSD component can be discriminated from those due to g-jitter if their frequencies are not overlapping. Recently, Kawaji (2003) studied the effect of g-jitter on the liquid bridge of middle *Pr* fluid (acetone) to find their negligible effect on the onset of oscillation.

2.3.2 Non-harmonic g-jitter

DSD measurements are done in the presence of non-harmonic g-jitter of amplitude spectra as shown in Fig. 16. This condition should provide more realistic case for future ISS experiment. Figure 18 shows the DSD signal measured in the presence of non-harmonic g-jitter. Note that the liquid bridge is in the sate of oscillation (ΔT=39K), thus exhibiting an oscillatory DSD at about 1Hz. The DSD signal also exhibits the components of higher frequencies due to g-jitter. In particular, the component of about 15Hz, which should be corresponding to the resonance frequency of the liquid bridge mentioned above, has a dominating amplitude. The amplitude spectrum of DSD measured is plotted in Fig. 19. It is seen that there are two sharp peaks at 1.25 and 2.5Hz, which should be corresponding to the natural DSD frequency and its second harmonics, respectively. There is another broad frequency range from 13.5 to 20.5Hz of significant amplitude. Comparison with the amplitude spectra of g-jitter shown in Fig. 16 indicates that the broad frequency range in DSD seen in Fig. 19 is likely due to the significant power of g-jitter imposed on the liquid bridge.

The results shown so far suggest that the natural DSD in the oscillatory state of the liquid bridge can be well separated from the DSD caused by g-jitters by an appropriate band-pass filtering of DSD signals measured. Although the choice of filtering frequency will be an important issue in the actual ISS experiment, it is determined to be 0.8-2.0Hz here. Figure 20 presents comparison of band-pass filtered DSD signals obtained in the absence and presence of g-jitter. Note that these results are obtained in separate experiments and therefore the conditions of the liquid bridge can be different slightly. Both DSD signals show nearly the same amplitude even though it is smaller than 0.1μm. Their frequencies are slightly different; it is about 0.75Hz in the absence of g-jitter while it is 0.85Hz in the presence of g-jitter. This difference can be attributed to the difference in the liquid-bridge conditions.

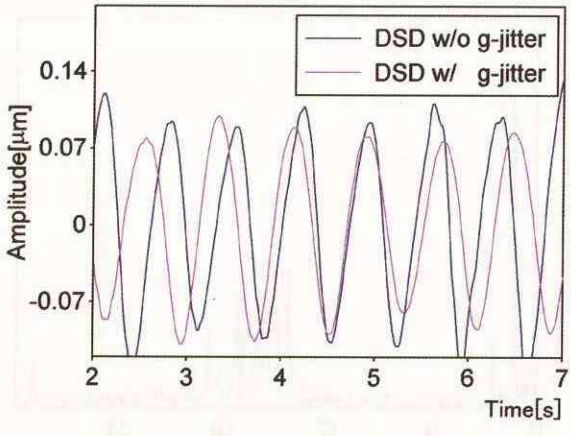

Fig. 20 Band-pass filtered DSD signals obtained in the absence and presence of g-jitter.

2.4 Conclusions of Chapter 2

Effects of g-jitter on the measurement of dynamic surface deformations (DSD) caused by the oscillatory thermocapillary convection in a liquid bridge have been studied experimentally. A vibration table driven by a piezoelectric actuator is constructed to generate g-jitters of realistic amplitude and frequency spectra. A micro-imaging displacement meter is used to measure DSD in the presence of g-jitter. It is shown that the natural DSD in the oscillatory state of thermocapillary convection is well separated in the frequency domain from that caused by harmonic and non-harmonic g-jitters. It is concluded that the DSD measurement in the future ISS experiment is feasible even in the presence of g-jitter there.

References

Cao, Z. H., You, X. T., Tang, Z. M. & Hu, W. R., 1001, Experimental investigation of thermocapillary convection in half floating zone, Advances in Space Research, Vol. 11, No. 7, p. 229.

Carlsson, T. E. & Wei, A., 2000, Phase evaluation of speckle patterns during continuous deformation by use of phase-shifting speckle interferometry, Applied Optics, Vol. 39, pp. 2628-2637.

Creath, K., 1985, Phase-shifting speckle interferometry, Applied Optics, Vol. 24, pp. 305-358.

Gustafsson, F., 1996, Determining the initial states in forward-backward filtering IEEE Transactions on Signal Processing, Vol. 44, No. 4, pp. 988-992.

Huntley, J. M., 2001, Automated analysis of speckle interferograms, *in* Digital Speckle Pattern Interferometry and Related Techniques, Rastogi, P. K. ed., Wiley, New York, pp. 59-139.

Joenathan, C., Franzec B., Haible, P. & Tiziani, H. J., 1998, Speckle interferometry with temporal phase evaluation for measuring large-object deformation, Applied Optics, Vol. 37, pp. 2608-2614.

Joenathan, C. & Torrba, R., 1991, Modified electronic speckle pattern interferometer employing an off-axis reference beam, Applied Optics, Vol. 30, pp. 1169-1171.

Jones, R. & Wykes, C., 1989, Holographic and speckle interferometry (2nd edition), Cambridge University Press.

Kamotani, Y. & Ostrach, S., 1998, Theoretical analysis of thermocapillary flow in cylindrical columns of high Prandtl number fluids, Transactions of the ASME, Journal of Heat Transfer, Vol. 120, pp. 758-764.

Kamotani, Y., Wang, L., Hatta, S., Bhunia, P. & Yoda, S., 2001, Study of oscillatory thermocapillary flow of high Prandtl number fluid, NASDA Technical Memorandum, NASDA-TMR-010015E, pp. 25-42.

Kawaji, M., 2003, private communication.

Kihm, K. D., 1997, Laser speckle photography technique applied for heat and mass transfer problem, Advances in Heat Transfer, Vol. 30, pp. 255-311.

Ko, H. S., Okamoto, K. & Madarame, H., 2001, Reconstruction of transient three-dimensional density distributions using digital speckle tomography, Measurement Science and Technology, Vol. 12, No. 8, pp. 1219-1226.

Kolenovic, E., Osten, W. & Jüptner, W., 1999, Non-linear speckle phase changes in the image plane caused by out of plane displacement, Optics Communications, Vol. 171, pp. 333-344.

Li, X., Tao, G. & Yang, Y., 2001, Continual deformation analysis with scanning phase method and time sequence phase method in temporal speckle pattern interferometry, Optics & Laser Technology, Vol. 33, 53-59.

Li, X., Soh, A.-K., Deng, B. & Guo, X., 2002, High-precision large deflection measurements of thin films using time sequence speckle pattern interferometry, Measurement Science and Technology, Vol. 13, No. 8, pp. 1304-1310.

Li, X. & Tao, G., 2002, Low-frequency harmonic vibration analysis with temporal speckle interferometry, Optics & Laser Technology, Vol. 34, pp. 259-264.

Madajarova, V. D., Kadano, H. & Toyooka, S., 2003, Dynamic electronic speckle pattern interferometry (DESPI) phase analyses with temporal Hilbert transformation, Optics Experss., Vol. 11, No. 6, pp. 617-623.

Nakadate, S. & Saito, H., 1985, Fringe scanning speckle-pattern interferometry, Applied Optics, Vol. 24, pp. 2172-2180.

Nishino, K., Kato, H. & Torii, K, 2000, Stereo imaging for simultaneous measurement of size and velocity of particles in dispersed two-phase flow, Measurement Science and Technology, Vol. 11, pp. 633-645.

Rastogi, P. K., 2001, Digital speckle pattern interferometry and related techniques, John Wiley & Sons, Ltd.

Roussev, I., Partalin, T., Toshev, E., Choulev, A. & Koulev, P., 1999, Digital speckle-metrology local investigation of sedimentation and surface effects in liquids, SPIE 3825, pp. 174-185.

Saldner, H. O., Molin, N. E. & Stetson, K. A., 1996, Fourier-transform evaluation of phase data in spatially phase-biased TV holograms, Applied Optics, Vol. 35, pp. 332-336.

Sanz, A. & Diez, J. L., 1989, Non-axisymmetric oscillations of liquid bridges, Vol. 205 , p. 503.

Takeda, M., 1990, Spatial-carrier fringe-pattern analysis and its applications to precision interferometry and profilometry: an overview, Ind. Metrology, Vol. 1, pp. 79-99.

Van der Auweraer, H., Steinbichler, H., Vanlanduit, S., Haberstok, C., Freymann, R., Storer, D. & Linet, V., 2002, Application of stroboscopic and pulsed-laser electronic speckle pattern interferometry (ESPI) to modal analysis problems, Measurement Science and Technology, Vol. 13, No. 4, pp. 451-463.

Verga, A., Baglioni, P., Dupont, O., Dewandel, J.-L., Beuselinck, T. & Bouwen, J., 1998, Use of electronic speckle pattern interferometers for the analysis of convective states of liquid in weightlessness, Optical Engineering, Vol. 37, No. 7, pp. 2161-2174.

Vikhagen, E., 1990, Nondestructive testing by use of TV holography and deformation phase gradient calculation, Applied Optics, Vol. 29, pp. 137-144.

Wang, J. & Grant, I., 1995, Electronic speckle interferometry, phase-mapping, and nondestructive testing techniques applied to real-time, thermal loading, Applied Optics, Vol. 34, pp. 3620-3627.

Wykes, C., 1982, Use of electronic speckle pattern interferometry (ESPI) in the measurement of static and dynamic surface displacements, Optical Engineering, Vol. 21, pp. 400-406.

Yao, Y. L., Liu, F. & Hu, W. R, 1996, How to determine critical Marangoni number in half floating zone convection, International Journal of Heat and Mass Transfer, Vol. 39, No. 12, p. 2539.

Yukawa, M., Nishino, K. & Torii, K., 2002, Mode structures of oscillatory Marangoni convection in a liquid bridge, CD-ROM Proceedings of the Tenth International Symposium on Flow Visualization, Paper F0330, Kyoto, Japan.